JOURNAL OF SPACECRAFT AND ROCKETS
Vol. 32, No. 2, March–April 1995

Spacecraft Low-Frequency Residual Acceleration

Hans Hamacher*
DLR, German Aerospace Research Establishment, Cologne, Germany

An analytical model is described to calculate the low-frequency acceleration, which is intended to replace the rather crude estimations applied to analyze previous Spacelab missions. The three principal low-frequency perturbations of the Space Shuttle Orbiter are taken into account: atmospheric drag, gravity gradient (tidal effect), and spacecraft rotation. These effects have been modeled on the basis of rigid-body dynamics, which requires a sufficient margin to the system's fundamental frequency f_f (1 Hz for the Orbiter-Spacelab combination). The calculation of the atmospheric drag is based on a dynamic model of the atmosphere that takes into account the diurnal (day-night) density variation. Gravity-gradient and rotational accelerations are calculated from the spacecraft attitude data. The main characteristics of the low-frequency accelerations are discussed on the basis of predicted data for Spacelab mission D-2.

Nomenclature

A_p	= spacecraft cross section projected normal to v_0
$\boldsymbol{a}$	= acceleration vector
C_d	= spacecraft drag coefficient
$\boldsymbol{d}$	= local vector between c.m. and P (Fig. 7)
F_d	= atmospheric drag force
$F_{10.7}$	= solar flux at 10.7-cm wavelength, W·s/m^2
f	= frequency
f_f	= spacecraft fundamental frequency
g_0	= Earth gravitational acceleration, 9.81 m/s^2
h	= orbit altitude
m	= spacecraft mass
v_0	= orbital velocity vector
(x, y, z)	= spacecraft-fixed coordinate system.
(x', y', z')	= coordinate system centered on c.m. (Fig. 7)
α	= right ascension
Δf	= difference between f_f and upper limit of rigid behavior (Fig. 2)
δ	= declination
λ	= constant lag angle, Fig. 4
ρ	= atmospheric density
ρ_0	= base density, Eq. (2)
ψ'	= angle between maximum of diurnal bulge and position of spacecraft, Eq. (4)
ω	= spacecraft angular velocity vector
ω_0	= orbital angular velocity vector

Subscripts

d	= drag
ext	= external
int	= internal
r	= rotational
s	= solar
t	= tidal

Introduction

A FREE-FALL system simulates weightlessness at its center of mass (c.m.), where gravity is locally canceled by inertia. This principle, approximated in a drifting spacecraft, is applied in space laboratories to carry out experiments under low-gravity conditions. The reason that complete weightlessness cannot be achieved in practice is one or several of the following deviations from the free-fall model:

1) Existing finite external forces cause the system to deviate from free fall. These forces originate from atmospheric drag, solar radiation pressure, any changes of the spacecraft total mass (e.g. due to thruster firings, mass dumps, outgassing or sublimation of materials), etc.

2) There are residual forces acting on objects that do not coincide with the c.m.: a) gravity is not completely canceled by intertia, on account of the gradient of the earth's gravitational field (tidal effect); b) any rotation of the spacecraft creates centrifugal and tangential forces.

3) Changes in the spacecraft mass allocation due to internal forces arise from running machines, crew activities, etc. Internal forces are always compensated in time and do not affect the motion of the spacecraft c.m.

The perturbing forces act on an interior object either directly as body forces (gravity, inertial forces) or indirectly as surface forces (all external and internal forces) via the spacecraft structure as illustrated in Fig. 1. The acceleration $\boldsymbol{a}$ of the object is thus determined by the time characteristics of the perturbing forces and the dynamic properties of the spacecraft structure. The frequency range of its dynamic response (Fig. 2) can be subdivided into two characteristic regimes with respect to f_f. In the range sufficiently below f_f the spacecraft behaves essentially like a rigid body (low-frequency range). The margin Δf between this range and f_f depends on the system's damping characteristics. For the case of the Space Shuttle Orbiter, f_f is close to 1 Hz as deduced from in-orbit acceleration measurements in various Spacelab missions.[1–4] The regime above $f_f - \Delta f$ is determined by the System's flexibility (high-frequency range). This is illustrated in Fig. 3, showing an example of frequency analysis deduced from measurements during Spacelab mission D1.[4] The symbols indicate the frequencies of system harmonics and excitation forces. Rigid behavior has been verified up to 0.3 Hz. The data in the low-frequency range have been estimated from orbit and attitude data. The reason for the lack of measured data is the deficiency in in-orbit calibration of the sensors. The zero offset is typically between 10^{-5} and $10^{-4} g_0$ for sensors applied to Spacelab acceleration measurement systems.

Only a very few systematic measurements exist in the low-frequency range, as a result of the complexity in performing in-orbit calibration.[5,6] There is, however, a strong demand for thorough and precise analyses, especially in the low-frequency range. This arises from investigations showing that the majority of physical phenomena are most sensitive to low-frequency acceleration.[7–11] The dashed lines in Fig. 3 are typical curves of the upper limit of continuous accelerations tolerated by experiments. The curves actually represent specified maxima of narrow-band residual acceleration allowed for the International Space Station Freedom (lower curve: routine disturbances; upper curve: schedulable events).

The computation of low-frequency accelerations thus plays an significant role in the characterization of the microgravity envi-

Received Oct. 23, 1992; revision received Sept. 6, 1993; accepted for publication Sept. 12, 1993.

*Professor, Aerospace Engineering.

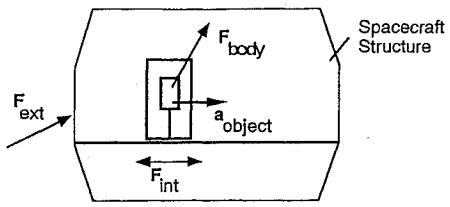

Fig. 1 Types of perturbing forces.

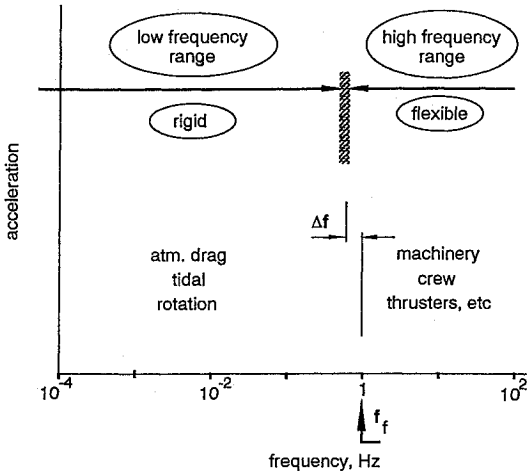

Fig. 2 Frequency regimes of residual acceleration for Spacelab.

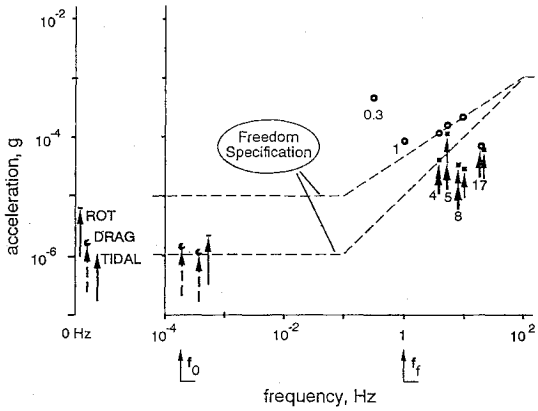

Fig. 3 Characteristic residual acceleration data of Spacelab D-1. Numbers indicate related frequencies.

ronment of a space laboratory. This paper describes an improved model for calculating the low-frequency accelerations to replace the rather crude estimations the experimenters had to rely on in previous Spacelab missions. The three principal perturbations causing low-frequency accelerations have been taken into account: 1) atmospheric drag, 2) the gravity-gradient (tidal) effect, and 3) slow spacecraft rotation. These effects are modeled on the basis of rigid-body dynamics. Special emphasis has been given to applying a dynamic atmospheric model to enhance the accuracy of drag data for the Space Shuttle Orbiter, which are given in the literature only on the basis of static models.[12] The application of the dynamic model also allows to determine the day-night (diurnal) variations of the atmospheric density and the related acceleration. This is of fundamental importance in analyzing the dynamics of the low-frequency acceleration vector. The calculation will be discussed on data calculated for the Spacelab mission D-2.

Low-Frequency Residual Accelerations

Atmospheric Drag

Atmospheric drag is the dominating external force for most vehicles flown in a low Earth orbit, such as the Orbiter and the Space Station Freedom. The force $\boldsymbol{F}_d$ is always directed opposite

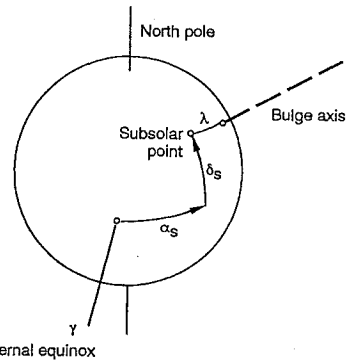

Fig. 4 Coordinates of the diurnal atmospheric bulge.

to v_0 and acts in the orbital plane. The magnitude of the related acceleration is given by

$$a_d = C_d(\rho/2)v^2(A_p/m) \tag{1}$$

Drag Coefficient

The coefficient C_d takes into account the spacecraft shape and the type of molecular interaction of the atmospheric species with the surface, e.g., diffusive or specular. It has been verified that, in a residual atmosphere rich in atomic oxygen, $C_d = 2.2$ can be taken with a maximum error[13] less than 10%. This situation obtains for altitudes within the thermosphere, where space laboratories are usually flown.

Atmospheric Density

For the calculation of ρ the explicit dynamic model by Jacchia[14] has been applied, which benefits from its closed mathematical form. The model takes into account the following density fluctuations:

1) The diurnal variation of ρ is attributed to the fact that the atmosphere bulges out in the general direction of the sun, with a pronounced lag caused by the earth's rotation. The density bulge is assumed to be axially symmetric with its geocentric latitude equal to the one of the subsolar point. Its longitude lags the sun by a constant lag angle of $\lambda = 25$–30 deg, as illustrated in Fig. 4.

2) Other density fluctuations are due to the 27-day effect, which is attributed to the sun's rotation, and 11-year cycle. These effects are correlated with the flux $F_{10.7}$ received at the 10.7-cm wavelength.

The actual density is obtained from the empirical relation

$$\rho = \rho_0(F_{10.7}/100)\{1 + 0.19[\exp(0.0055h) - 1.9]f(\psi')\} \tag{2}$$

where

$$\log \rho_0 = -16.021 - 1.985 \times 10^{-3}h + 6.363 \exp(-2.6 \times 10^{-3}h) \tag{3}$$

and

$$f(\psi') = \left(\frac{1 + \cos\psi'}{2}\right)^3 \tag{4}$$

with ρ_0 in g/cm^3, h in kilometers, and $F_{10.7}$ in W·s/m^2. The angle ψ' follows from the relation[12]

$$\cos\psi' = \sin\delta \sin\delta_s + \cos\delta \cos\delta_s \cos(\alpha - \alpha_s - \lambda) \tag{5}$$

The application of Eq. (2) is intended to describe the diurnal variation over a time period of a few hours, which represents the running time of a typical Spacelab experiment. The parameters ρ_0 and $F_{10.7}$ can be considered constant during this period. Figure 5 shows the diurnal density variation as calculated for $h = 300$ km and the sun's latitude of $\delta_s = 23.5$ deg. This example shows a diurnal density variation along one orbit of approximately 50%.

Effective Cross Section

Most spacecraft have complex shapes for which the cross-sectional areas are known for few axes only. In the case of the Orbiter, the cross sections are given for the three principal axes as shown in Fig. 6. In the application of this model the Orbiter has been represented by a cuboid.

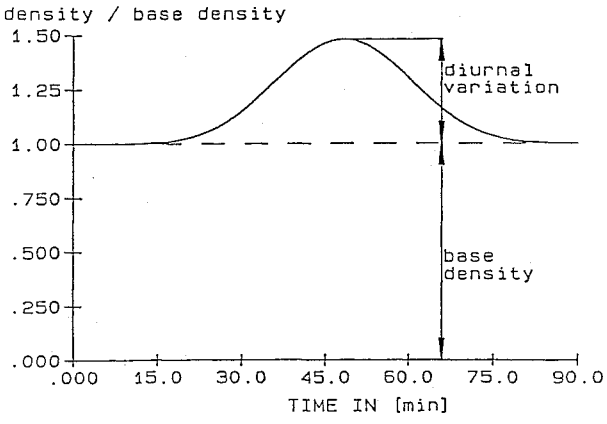

Fig. 5 Diurnal density variation for $h = 300$ km, $\delta_s = 23.5$ deg, $\psi = 0$, and $F_{10.7} = 150 \times 10^{-22}$ W· s/m^2.

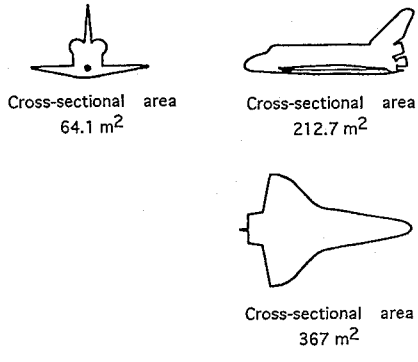

Fig. 6 Cross-sectional areas of the Orbiter for the three principal axes.

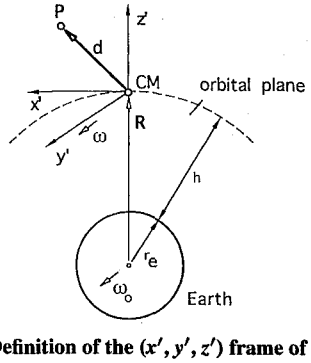

Fig. 7 Definition of the (x', y', z') frame of reference.

Tidal Effect

The tidal acceleration $\boldsymbol{a}_t$ is proportional to the local vector $\boldsymbol{d}(x', y', z')$ between the c.m. and the location P (Fig. 7). For the frame of reference (x', y', z') centered at the c.m. with the x' and z' axes in the orbital plane and z' pointing at the zenith, $\boldsymbol{a}_t$ is given by

$$\boldsymbol{a}_t = \omega_0^2 \begin{Bmatrix} -1 & 0 & 0 \\ 0 & -1 & 0 \\ 0 & 0 & 2 \end{Bmatrix} \begin{Bmatrix} x' \\ y' \\ z' \end{Bmatrix} \tag{6}$$

where ω_0 is known from orbit data.[15] The calculation also requires knowledge of the various experiment locations $\boldsymbol{d}$ relative to the c.m.

Rotational Acceleration

In a similar way the rotational acceleration $\boldsymbol{a}_r$ follows for a given location $\boldsymbol{d}(x, y, z)$ from

$$\boldsymbol{a}_r = \boldsymbol{\omega} \times (\boldsymbol{\omega} \times \boldsymbol{d}) + \frac{\mathrm{d}}{\mathrm{dt}}(\boldsymbol{\omega} \times \boldsymbol{d}) \tag{7}$$

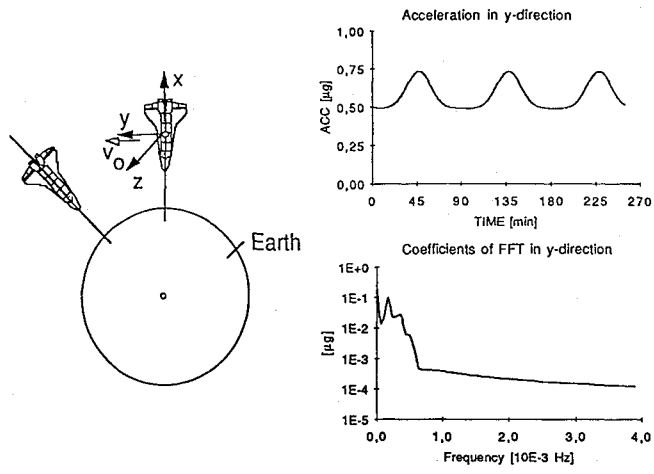

Fig. 8 Acceleration and frequency spectrum for gravity-gradient attitude in y-(flight) direction.

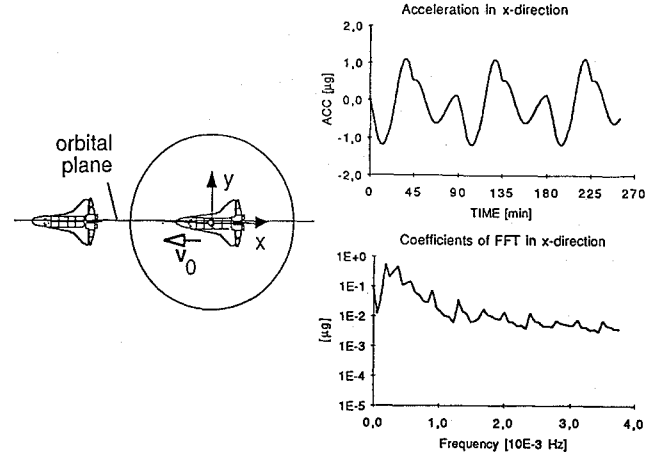

Fig. 9 Acceleration and frequency spectrum for inertial attitude in x direction.

Case Study: Spacelab Mission D-2

Attitudes and Orbit Parameters

The low-frequency acceleration will be calculated for the following three typical mission phases of Spacelab D-2:

1) *Gravity gradient attitude.* The microgravity-oriented missions like D-2 are preferably flown in a gravity-gradient-stabilized attitude (Fig. 8).

2) *Inertial attitude.* Another dominating attitude is the inertial hold of the spacecraft (Fig. 9).

3) *Maneuvers* for attitude changes of the Orbiter are executed with a standard rotation rate of 0.2 deg/s, i.e., one revolution in 30 min. A typical maneuver will be discussed in Fig. 10.

The data have been calculated from the location $\boldsymbol{P}(x = -2.2$ m, $y = 0$, $z = 2.2$ m) in the Spacelab coordinates defined in Fig. 8, which represents the distance of a typical D-2 experiment from the Orbiter's c.m. The calculation is based on the following parameters given in Table 1.

Discussion

Gravity-Gradient Attitude

The modulation of the residual acceleration in the flight (y) direction is shown in Fig. 8. It reflects essentially the diurnal density variation of Fig. 5, which was calculated for this set of orbit parameters. The dc value is close to $6 \times 10^{-7} g_0$. Pronounced peaks in the amplitude spectrum appear at the orbital frequency $f_0 = 1.9 \times 10^{-4}$ Hz ($1 \times 10^{-6} g_0$), and at its first harmonic at 3.8×10^{-4} Hz ($3 \times 10^{-7} g_0$). The amplitudes attenuate rapidly towards higher frequencies. They are below $10^{-9} g_0$ at frequencies above the fourth harmonic. The accelerations in the x and the z direction are constant except for earth oblateness effects, which cause errors of the order of 10^{-3}.

Table 1 Parameters for the example calculation

Altitude	$h = 300$ km
Orbital frequency	$f_0 = 1.9 \times 10^{-4}$ Hz
Spacecraft mass	$m = 90 \times 10^3$ kg
Drag coefficient	$C_d = 2.3$
Orbit inclination	$i = 28.5$ deg
Subsolar point	$\alpha_s = 90$ deg, $\delta_s = 23.5$ deg
Solar flux parameter	$F_{10.7} = 150 \times 10^{-22}$W· s/m^2
Start time	Midnight at $\delta = 0$ longitude
Number of orbits analyzed	3

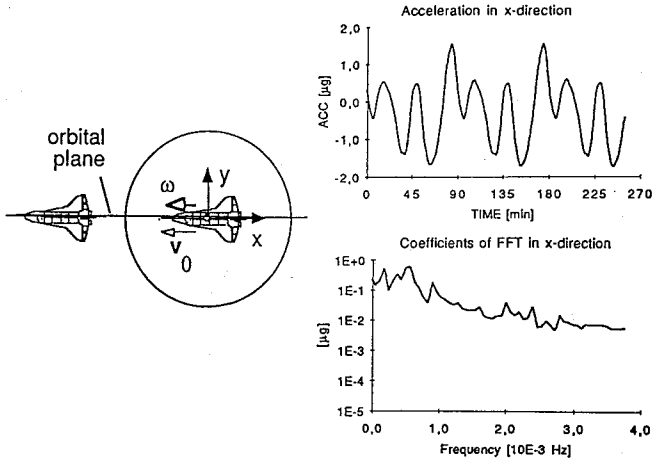

Fig. 10 Acceleration and frequency spectrum for inertial attitude, x axis in orbital plane, and ω parallel to x axis.

Inertial Attitude

The residual acceleration in the time domain (Fig. 9) reflects the superposition of drag and tidal acceleration. The vector of atmospheric drag, $\boldsymbol{F}_d$, rotates once per orbit relative to the spacecraft. This and the variation of A_p and ρ in Eq. (1) are the reasons for the pronounced amplitude at f_0 in the x direction. The finite dc value originates from the diurnal change, the only parameter that is uncompensated over the orbit. The tidal vector varies harmonically with a frequency twice the orbital frequency f_0, which is reflected in the spectrum.[15] The attenuation of the amplitudes is weaker than for the gravity-gradient attitude, but is still two orders of magnitude between dc and 2×10^{-3} Hz. The spectra for the x and z components are identical.

Maneuver

The effect of a standard roll maneuver was analyzed for the case of inertial hold of the x axis superimposed on a rotation vector ω parallel to the x axis. As was to be expected, the maxima in the time and frequency domains are the highest among the three cases discussed. The centrifugal acceleration in a standard maneuver always dominates the low-frequency acceleration. The same result was found in the analysis of the D-1 data as shown in Fig. 3.

Conclusions

The application of the analytical approach described in this paper reveals strong variations of the residual accelerations in the low-frequency range. The atmospheric drag shows a variation of about 50% over one orbit in the case discussed for Spacelab mission D-2.

The calculation of the tidal and the rotational acceleration relies on attitude data, which are measured with high accuracy for the Orbiter. The distance $\boldsymbol{d}$ in Eqs. (6) and (7), however, is difficult to determine, primarily because of the c.m. shift that results from mass losses (fuel consumption, water dumps, etc.) during the mission. Estimated data on the c.m. position are available.

The analysis of the three D-2 mission phases show that the spectrum for the gravity-gradient mode attenuates fairly rapidly towards higher frequencies. The attenuation is weakest for the standard maneuver. These results are not only of interest to the analysis of microgravity experiments. They are also important criteria for the design and optimization of experiment hardware. They are of special interest for the design of microgravity isolation mounts.[16]

Acknowledgment

The author is indebted to Michael Kesselmann, Technical University of Munich, and Udo Bluemel, DLR, for their valuable support in the programming and calculation of the data.

References

[1]Rogers, M. J. B., and Alexander, J. I. D., "Residual Acceleration Data Analysis for Spacelab Missions," *Microgravity Science and Technology*, Vol. V, No. 1, 1992, pp. 43–49.

[2]Hamacher, H., and Merbold, U., "Microgravity Environment of the Materials Science Double Rack on Spacelab-1," *Journal of Spacecraft and Rockets*, Vol. 24, No. 3, 1987, pp. 264–269.

[3]Martin, G. L., Baugher, C. R., and Henderson, F. H., "Summary Report of Mission Acceleration Measurements STS-50," Space Science Lab., NASA/Marshall Space Flight Center, NASA-ACAP, Nov. 1992.

[4]Hamacher, H., Jilg, R., and Merbold, U., "Analysis of Microgravity Measurements Performed During D1," ESA SP-256, Feb. 1987, pp. 413–420.

[5]Blanchard, R. C., Nicholson, J. Y., and Ritter, J. R., "Absolute Acceleration Measurements on STS-50 from the Orbital Acceleration Research Experiment (OARE)," in *Microgravity Science and Technology* (to be published).

[6]Hamacher, H., Jilg, R., and Feuerbacher, B., "QSAM—A Measurement System to Detect Quasi-Steady Accelerations Aboard a Spacecraft," *International Astronautical Federation*, Paper 90-377, Oct. 1990, pp. 1–7.

[7]Alexander, J. I. D., "Low Gravity Experiment Sensitivity to Residual Acceleration: A Review," *Microgravity Science and Technology*, Vol. 3, pp. 52–68, 1990.

[8]Naumann, R. J. "Susceptibility of Materials Processing Experiments to Low Level Acceleration," *Proceedings on Spacecraft Dynamics as Related to Laboratory Experiments in Space*, NASA Marshall Space Flight Center, May 1979, NASA CP 2199, May 1981, pp. 184–194.

[9]Langbein, D., and Tiby, C., "Allowable g-Levels for Microgravity Payloads," Final Report for ESA, Batelle Frankfurt, Sept. 1984, pp. 1–24.

[10]Monti, R., Langbein, D., and Favier, J. J. "Influence of Residual Accelerations on Fluid Physics and Materials Science Experiments," *Fluid Sciences and Materials Science in Space*, edited by H. U. Walter, Springer–Verlag, Berlin, 1987, pp. 637–680.

[11]Feuerbacher, B., Hamacher, H., and Jilg, R., "Compatibility of Microgravity Experiments with Spacecraft Disturbances," *Zeitschrift für Flugwissenschaften und Weltraumforschung*, Vol. 12, pp. 145–151, 1988.

[12]Anon., *Spacelab Payload Accommodation Handbook*, NASA SPL/2104, Aug. 1985.

[13]King-Hele, D. G., *Satellite Orbits in an Atmosphere: Theory and Applications*, Blackie, Glasgow and London, 1987.

[14]Jacchia, L. G., "Variations in the Earth's Upper Atmosphere as Revealed by Satellite Drag," *Reviews of Modern Physics*, Vol. 35, No. 4, 1963, pp. 973–991.

[15]Hamacher, H., Fitton, B., and Kingdon, J., "The Environment of Earth-Orbiting Systems," *Fluid Sciences and Materials Science in Space*, edited by H. U. Walter, Springer–Verlag, Berlin, 1987, pp. 1–50.

[16]Jones, D. I., Owens, A. R., and Owen, R. G., "A Microgravity Isolation Mount," Paper 86-270, Oct. 1986.

E. A. Thornton
Associate Editor